EPJ manuscript No.
(will be inserted by the editor)

Molecular dynamics simulation for the baryon-quark phase transition at finite temperature and density

Yuka Akimura[1,2], Toshiki Maruyama[2], Naotaka Yoshinaga[1], and Satoshi Chiba[2]

[1] Department of physics, Saitama University, 255 Shimo-Okubo, Sakura-Ku, Saitama City, Saitama 338-8570, Japan, e-mail: akimura@tiger04.tokai.jaeri.go.jp
[2] Advanced Science Research Center, Japan Atomic Energy Research Institute, Tokai, Ibaraki 319-1195, Japan

Received: date / Revised version: date

Abstract. We study the baryon-quark phase transition in a molecular dynamics (MD) of quark degrees of freedom at finite temperature and density. The baryon state at low density and temperature, and the deconfined quark state at high density and temperature are reproduced. We investigate the equations of state of matters with different *u*-*d*-*s* compositions. Then we draw phase diagrams in the temperature-density plane by this simulation. It is found that the baryon-quark transition is sensitive to the quark width.

PACS. PACS-key discribing text of that key – PACS-key discribing text of that key

1 Introduction

It is expected that quarks are observed as deconfined states at extreme environment: at high density and/or high temperature, where baryons or thermal pions overlap with each other, disappearance of hadron boundaries may give rise to the quark gluon plasma (QGP). Also the change of coupling constants and the quark mass due to the nature of the quantum chromodynamics (QCD), is thought to be one of the origins of the QGP [1]. Recently many theoretical calculations are attempted to draw a QCD phase diagram [2,3,4]. The critical temperature of the hadron-quark phase transition is predicted to be around 150 MeV by lattice simulations [5,6]. For a finite density system, the bag model predicts in a qualitative study [7] that the critical density lies at a few times the normal nuclear saturation density. Many efforts are devoted to experimental search for the QGP by using high energy accelerators. There, many indirect signals of the QGP have been observed [8,9,10] but a definite conclusion has not been obtained since theoretical studies are not enough to characterize the properties of the QGP and hadron gas at present. It is not clear how hadron matter changes to quark matter and how the physical property changes at the hadron-quark transition.

The Lattice simulation based on the first principle is the most reliable method for QCD. It has been applied to high-temperature and low-density systems under some approximations. At high density, however, the complex fermion determinant, or the sign problem, makes the simulation practically impossible [11]. One of the approaches for treating finite density systems is a mean field theory which makes the most of its ability for uniform systems. There are many works with the mean field treatment, which are incorporated with the chiral restoration by the Nambu-Jona-Lasinio model [12], the bag model picture [13], the soliton model picture [14], and so on. The dynamics of hadron-quark transition, however, are not considered in these cases. In these circumstances, other approaches which are feasible for treating the finite density and the dynamics are being awaited.

The molecular dynamics (MD) has been successful in treating many-body nucleon systems. To describe the structure and the dynamics of many-body nucleon systems, several MD models were proposed [15,16,17,18] and obtained some remarkable results. Advantages of the MD simulation are that one needs very few assumptions a priori and that a single model can be applied to various problems. To investigate properties of hadron and quark matter and the dynamics of transition between these two phases in a unified manner, MD is a natural framework to be attempted. In this paper we apply a model similar to quantum molecular dynamics (QMD) [15] to many-body quark systems, within a framework of the non-relativistic quark model. Some pioneering works of applying MD to quark systems were presented where transitions caused by increasing density and temperature were studied in the view point of many-body dynamics: in [19,20] the Vlasov equation and the Vlasov+MD approach were used to ge t the equation of state of matter. In [21] quark MD was applied to heavy-ion collisions where the creation of particle-antiparticle pairs was taken into account. In [22], the color gauge symmetry was treated exactly and the meson exchange potentials were introduced. In the above studies quarks were treated as classical particles and there was

ambiguity in the definition of the ground state of the system. In the present paper, we propose a model which has less ambiguity to describe the ground state and to define the temperature. With this model we study the mechanism of the baryon-quark transition and draw the phase diagram together with the equation of state (EOS) for a wide range of baryon density and temperature.

This paper is organized as follows. In section 2 we explain basics of the model in detail. Simulation results for the three kinds of matters: *ud* (matter containing the same number of u and d quarks; corresponds to symmetric nuclear matter), *udd* (d quarks twice the number of u quarks; neutron matter) and *uds* (the same number of u, d and s quarks; Λ matter) by using two kinds of quark width are given in section 3. In section 4 we apply the model to finite temperature systems and present phase diagrams. Summary is given in section 5.

2 molecular dynamics for quark matter

2.1 Wave functions and cooling equations

We start with the total wave function by a direct product of $n = 3A$ single particle quark Gaussian wave packets in coordinate and momentum spaces and state vectors χ with a fixed flavor, a color and a spin orientation,

$$\Psi = \prod_{i=1}^{n} \frac{1}{(\pi L^2)^{3/4}} \exp\left[-\frac{(\mathbf{r}_i - \mathbf{R}_i)^2}{2L^2} + \frac{i}{\hbar}\mathbf{P}_i\mathbf{r}_i\right]\chi_i, \quad (1)$$

where $n = 3A$ (A is the baryon number), L the fixed width of wave packets, and $\mathbf{R}_i$ and $\mathbf{P}_i$ are the center of the wave packet of i-th quark in coordinate and momentum spaces, respectively. Instead of antisymmetrization of the total wave function, the fermionic nature of the system is phenomenologically treated by introducing the Pauli potential which acts repulsively between quarks having the same flavor, color and spin orientation [23]. The equations of motion for $\mathbf{R}_i$ and $\mathbf{P}_i$ are given by the Newtonian equations,

$$\dot{\mathbf{R}}_i = \frac{\partial H}{\partial \mathbf{P}_i}, \quad \dot{\mathbf{P}}_i = -\frac{\partial H}{\partial \mathbf{R}_i}. \quad (2)$$

When we search for the ground state (energy minimum configuration) of the system, we solve the equations of motion with friction terms, which we call "cooling equations of motion",

$$\dot{\mathbf{R}}_i = \frac{\partial H}{\partial \mathbf{P}_i} + \mu_r\frac{\partial H}{\partial \mathbf{R}_i}, \quad \dot{\mathbf{P}}_i = -\frac{\partial H}{\partial \mathbf{R}_i} + \mu_p\frac{\partial H}{\partial \mathbf{P}_i}, \quad (3)$$

where μ_r and μ_p are negative frictional coefficients. The cooling is performed until the particles stop ($\dot{\mathbf{R}}_i = 0$). In the ground state, the momenta $\mathbf{P}_i$ have finite values because of the momentum dependence of the Pauli potential.

In order to simulate the infinite system (matter) by using a finite number of quarks, we use a cubic cell with 26 mirroring cells under a periodic boundary condition. The cell size is chosen to be 6 fm throughout this paper.

2.2 Effective Hamiltonian

The effective Hamiltonian consists of three parts as,

$$H = H_0 + V_{\rm Pauli} - T_{\rm spur}, \quad (4)$$

where H_0 is the original Hamiltonian expressed as

$$H_0 \equiv \left\langle \Psi \left| \sum_{i=1}^{n} \hat{T}_i + \hat{V}_{\rm color} + \hat{V}_{\rm meson} \right| \Psi \right\rangle, \quad (5)$$

$$E_i \equiv \left\langle \Psi \left| \hat{T}_i \right| \Psi \right\rangle = \frac{\mathbf{P}_i^2}{2m_i} + \frac{3\hbar^2}{4m_iL^2} + m_i. \quad (6)$$

We employ the quark-quark interactions as follows,

$$\hat{V}_{\rm color} = \frac{1}{2}\sum_{i=1,j\neq i}^{n}\left(-\sum_{a=1}^{8}\frac{\lambda_i^a\lambda_j^a}{4}\left(K\hat{r}_{ij} - \frac{\alpha_s}{\hat{r}_{ij}}\right)\right), \quad (7)$$

$$\begin{aligned}\hat{V}_{\rm meson} = \sum_{i=1,i\in l}^{n}\Bigg[&\frac{1}{2-\varepsilon}\left(-\frac{g_{\sigma q}^2}{4\pi}\right)\left(\sum_{j\neq i,j\in l}^{n}\frac{e^{-\mu_\sigma\hat{r}_{ij}}}{\hat{r}_{ij}}\right)^{1-\varepsilon} \\ &+ \frac{1}{2}\sum_{j\neq i,j\in l}^{n}\left(\frac{g_{\omega q}^2}{4\pi}\frac{e^{-\mu_\omega\hat{r}_{ij}}}{\hat{r}_{ij}} + \frac{\sigma_i^3\sigma_j^3}{4}\frac{g_{\rho q}^2}{4\pi}\frac{e^{-\mu_\rho\hat{r}_{ij}}}{\hat{r}_{ij}}\right)\Bigg] \\ &+ \frac{1}{2}\sum_{i=1,i\in s}^{n}\sum_{j\neq i,j\in s}^{n}\frac{g_{\phi q}^2}{4\pi}\frac{e^{-\mu_\phi\hat{r}_{ij}}}{\hat{r}_{ij}}, \end{aligned} \quad (8)$$

where $\hat{r}_{ij} \equiv |\mathbf{r}_i - \mathbf{r}_j|$ and l means a light flavor u or d. The color dependent interaction $\hat{V}_{\rm color}$ consists of the linear confining potential with an infrared cut-off at 3 fm and the one gluon exchange potential [22] with Gell-Mann matrices λ^a. To include the antisymmetric effect for the matrix elements of color space, we use effective values of $\langle\chi_i|\lambda_i^a\lambda_j^a|\chi_j\rangle^{\rm eff} = 4\langle\chi_i|\lambda_i^a\lambda_j^a|\chi_j\rangle$ [22]. The color force is approximately canceled between a colored quark and a white baryon made of quarks with three colors locating near to each other. $\hat{V}_{\rm meson}$ consists of σ, ω and ρ meson exchange potentials which act among light flavor quarks (u quarks and d quarks), and the ϕ meson exchange potential which acts among s quarks, where σ^3 is the third component of Pauli matrices. We modify the σ exchange potential of Yukawa-type with a small non-linearity parameter ε. This corresponds to a density dependent potential or a method in the relativistic mean field theory (RMF) where higher order terms in σ field are introduced to reproduce the saturation property for the symmetric nuclear matter. For simplicity, we have written Eq. (8) in the form of an operator. In practice, however, the power by $1-\varepsilon$ of the σ exchange potential is performed after evaluating the expectation value. The parameters in the meson exchange potentials are adjusted to reproduce the baryon-baryon interactions as described in Sec. 2 C.

Lack of the antisymmetrization is compensated by using the Pauli potential,

$$V_{\rm Pauli} = \frac{C_p}{(q_0p_0)^3}\exp\left[-\frac{(\mathbf{R}_i - \mathbf{R}_j)^2}{2q_0^2} - \frac{(\mathbf{P}_i - \mathbf{P}_j)^2}{2p_0^2}\right]\delta_{\chi_i\chi_j}, \quad (9)$$

where q_0, p_0 and C_p are parameters determined in Sec. 2 C. Antisymmetrized wave functions are not used because it takes CPU time proportional to the forth power of a particle number [16,17]. On the other hand, MD without antisymmetrization needs CPU times proportional to the second power of the particle number. At present, simulation with antisymmetrization is not practically possible for the system with several hundreds of particles. Furthermore, the way to antisymmetrize wave functions with a periodic boundary condition has not been established yet. We have to subtract the spurious zero point energy of the center-of-mass motion of clusters [17,18],

$$T_{\rm spur} = \sum_{i=1}^{n} \frac{3\hbar^2}{4m_i L^2} \frac{1}{M_i}, \tag{10}$$

$$M_i \equiv \sum_{j=1}^{n} f_{ij}, \tag{11}$$

$$f_{ij} \equiv \begin{cases} 1 & (R_{ij} \le a_f) \\ \exp\left[-\frac{(R_{ij}-a_f)^2}{w_f^2}\right] & (R_{ij} > a_f) \end{cases}, \tag{12}$$

where $R_{ij} \equiv |\mathbf{R}_i - \mathbf{R}_j|$ and M_i is the "mass number" of fragment to which the wave packet i belongs, which is the sum of "friendship" f_{ij} with other particles. To apply the model to various densities, we introduce a density-normalized parameters of cluster separation in the friendship as

$$a_f = a_0 \left(\frac{\rho_0}{\rho}\right)^{1/3}, \quad w_f = w_0 \left(\frac{\rho_0}{\rho}\right)^{1/3}, \tag{13}$$

where ρ_0 means the normal nuclear density 0.17 fm^{-3}.

2.3 Choice of parameters

2.3.1 Quark model parameter and friendship

We use the constituent quark mass $m_{u,d} = 300$ MeV for light quarks and $m_s = 500$ MeV for s quarks throughout this simulation. For the color potential, 900 MeV/fm is used for the string tension K and 1.25 for the QCD fine structure constant α_s, which are typical in quark models [24].

The parameters in the friendship are chosen as $a_0 = 0.3$ fm and $w_0 = 0.5$ fm, so that the sum of the friendship $M_i \approx 3$ when the system clusterizes as baryons and $M_i \approx 1$ when quarks do not make clusters.

The width of quarks L is the most important parameter in this model since it is directly related to the density at which baryon-quark transition occurs. We use two different widths by considering the masses of isolated nucleon N and lambda particle Λ. To minimize the energy (mass) of a nucleon, L becomes 0.43 fm. However, the nucleon mass is too large (about 2400 MeV) with this value of L. The reason of this overestimation is that the ground-state kinetic energy per quark in a nucleon, $\frac{2}{3}\frac{3\hbar^2}{4m_{u,d}L^2}$, has a large value of 351 MeV, while the kinetic energy of a quark in a nucleon is roughly estimated to be 50 – 80 MeV from the uncertainty principle. Therefore, we employ "effective" widths $L^{\rm eff}$ in evaluating E_i (Eq. (6)) and $T_{\rm spur}$ (Eq. (10)). The ground-state kinetic energy per quark in a nucleon becomes 65 MeV if we use $L^{\rm eff} = 1.0$ fm.

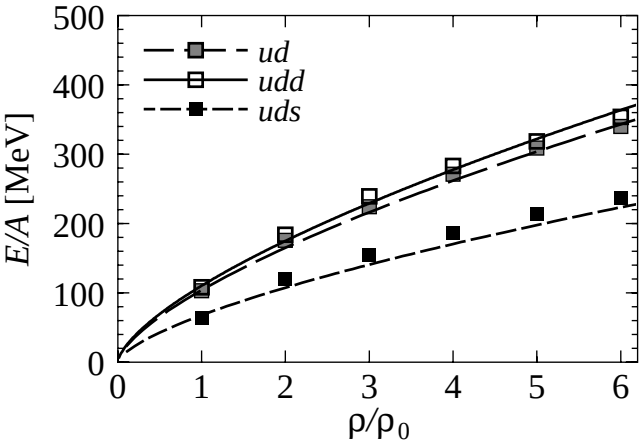

Fig. 1. Energy per baryon of free Fermi gas. The lines show the theoretical exact values of ud, udd and uds matter. The marks are the kinetic energies calculated by MD with only the Pauli potential.

Our first choice is to use $L = 0.43$ fm, $L^{\rm eff}_{u,d} = 1.0$ fm and $L^{\rm eff}_s = 0.8$ fm. We call this choice as "width parameter (I)". This combination still gives a slightly large value of the nucleon mass, $M_N \approx 1500$ MeV, but gives a proper difference of masses between N and Λ.

Once the effective width $L^{\rm eff}$ for kinetic energy is employed, the nucleon mass does not have a minimum regarding L. Then the second choice is made to give a proper nucleon mass value, $M_N \approx 940$ MeV by changing L to be 0.33 fm (but with the same values of $L^{\rm eff}$ as before). In this case, the difference of masses between N and Λ cannot be set to a desired value. We call this choice as "width parameter (II)".

2.3.2 Pauli potential

For the Pauli potential, the parameters C_p, q_0, p_0 are determined by fitting the kinetic energy to the exact Fermi gas at zero temperature. We determine these values by solving the cooling equation (3) for ud matter, udd matter and uds matter where only the Pauli potential is considered [23]. Figure 1 shows the classical and non-relativistic kinetic energy of the Fermi gas. The lines indicate the values of the exact Fermi gas energy for ud matter, udd matter and uds matter. The squares show the kinetic energy of each matter, whose values are obtained by using following parameters: we adopt $q_0 = 1.6$ fm, $p_0 = 120$ MeV and $C_p = 131$ MeV for light quarks and $C_p = 79$ MeV for s quarks. Here three different colors and two different spins are assumed for each matter. It is seen that the difference between ud matter and udd matter is small. By introducing heavy s quarks, the Fermi energy of uds

matter becomes lower than that of ud matter. Note that the Pauli potential gives a spurious potential energy to the system, which should be renormalized into other effective potential terms [23]. One possibility to avoid this problem is, instead of using the Pauli potential, to maintain the Pauli principle of the system by stochastic rearrangements of particle momenta [25]. This model was originally developed for nucleon systems and was applied also to the quark system very recently [26].

2.3.3 Meson exchange potentials

Though the meson exchange potentials do not affect the baryon-quark transition, we adjust the meson exchange potentials to discuss the EOS of strange and normal nuclear matters. Prameters are determined to get appropriate ground state energy of "baryon matter" by frictional cooling with a constraint that quarks form baryon clusters (baryonization constraint). First we randomly distribute baryons which are composed of three quarks and solve the cooling equation with the baryonization constraint as,

$$\dot{\mathbf{R}}_i = \frac{1}{3}\sum_{j\in\{i\}}\left[\frac{\partial H}{\partial \mathbf{P}_j} + \mu_r \frac{\partial H}{\partial \mathbf{R}_j}\right],$$
$$\dot{\mathbf{P}}_i = \frac{1}{3}\sum_{j\in\{i\}}\left[-\frac{\partial H}{\partial \mathbf{R}_j} + \mu_p \frac{\partial H}{\partial \mathbf{P}_j}\right], \qquad (14)$$

here $\{i\}$ means a set of three quarks in a baryon to which i-th quark belongs [22]. We call this cooling "baryon cooling". In Fig. 2 baryon density dependence of the energy per baryon is shown for ud matter (corresponding to symmetric nuclear matter), udd matter (neutron matter) and uds matter (Λ matter). Note that in this calculation with the baryonization constraint, the color-dependent interactions are exactly canceled between the white baryons. For the σ exchange potential, $g_{\sigma q} = 3.09$, $m_\sigma = 400$ MeV, $L_\sigma = 1.2$ fm and $\varepsilon = 0.1$ are used and $g_{\omega q} = 4.98$, $m_\omega = 782$ MeV and $L_\omega = 0.7$ fm for the ω ex change and $g_{\rho q} = 9.0$, $m_\rho = 770$ MeV and $L_\rho = 1.2$ fm for the ρ exchange potential. In order to reproduce the well-known properties of matter, we have introduced the effective widths for each meson exchange term. We fit the binding energy of ud matter to 16.5 MeV/nucleon at $1\rho_0$. The EOS of Λ matter, which depends on the ϕ exchange potential is unsettled yet [27]. In order to obtain the saturation of uds matter, we need to introduce an attractive K exchange interaction between u-s or d-s quarks. However the K meson exchange is prohibited according to the RMF model. Here we have only a repulsive ϕ exchange interaction between s quarks for simplicity. The relevant parameters are $g_{\phi q} = \sqrt{2} g_{\omega q} = 7.04$ [27], $m_\phi = 1020$ MeV and $L_\phi = 0.7$ fm. Even if we use another value, e.g. $L_\phi \sim 1$ fm, the behavior of the EOS is not changed noticeably.

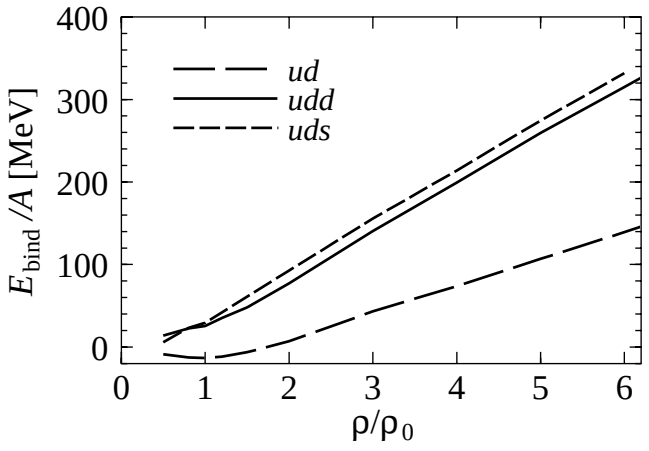

Fig. 2. Binding energies per baryon for ud, udd and uds matter calculated by the baryon cooling. The saturation is seen for the ud matter, but it is not seen for the udd and uds matter.

3 Results for the finite density system

Here we investigate the stability and the structure of quark matter in the ground stat e (zero temperature) for a wide range of density. We solve the cooling equations (3) with quark degrees of freedom. We call this cooling "quark cooling" in contrast to the baryon cooling. Snapshots of the ground state of uds matter with the width parameter (I) (L=0.43 fm) are displayed in Fig. 3. Three quarks in red, green and blue located within a distance $d_{\rm cluster}$ are considered to be confined as a baryon

$$\begin{aligned} &|\mathbf{R}_i - \mathbf{R}_j| < d_{\rm cluster}, \\ &|\mathbf{R}_j - \mathbf{R}_k| < d_{\rm cluster}, \\ &|\mathbf{R}_k - \mathbf{R}_i| < d_{\rm cluster}, \\ &\quad \{i,j,k\} = \{\text{red}, \text{green}, \text{blue}\}, \end{aligned} \qquad (15)$$

where we use $d_{\rm cluster} = 0.7$ fm. Quarks judged to be in a confined state are plotted in white and those deconfined in its own color. At the normal baryon density $1\rho_0$ all quarks are confined as baryons. As density increases, some quarks become deconfined and the confined and the deconfined states coexist around $2.5\rho_0$. Most of the quarks are deconfined at high baryon density $\rho \geq 3\rho_0$. The ground state energies of ud, udd and uds matters with the width parameter (I) are shown by solid lines in Fig. 4. The vertical axis indicates the energy per baryon. For comparison, the case of baryon cooling is shown by thin dashed lines. The energy by quark cooling agrees with that by baryon cooling at low density. This means that quarks are confined as baryons. At a certain density, a baryon-quark transition occurs and the energy decreases. The mechanism of baryon-quark transition in our dynamical model is as follows. If confined quarks are released from a baryon, their kinetic energy, most of which has been the zero point energy, decreases. On the other hand, the potential energy increases due to the confinement force. At above a certain density, the increase of potential energy at deconfinement gets smaller due to the existence of many other quarks in

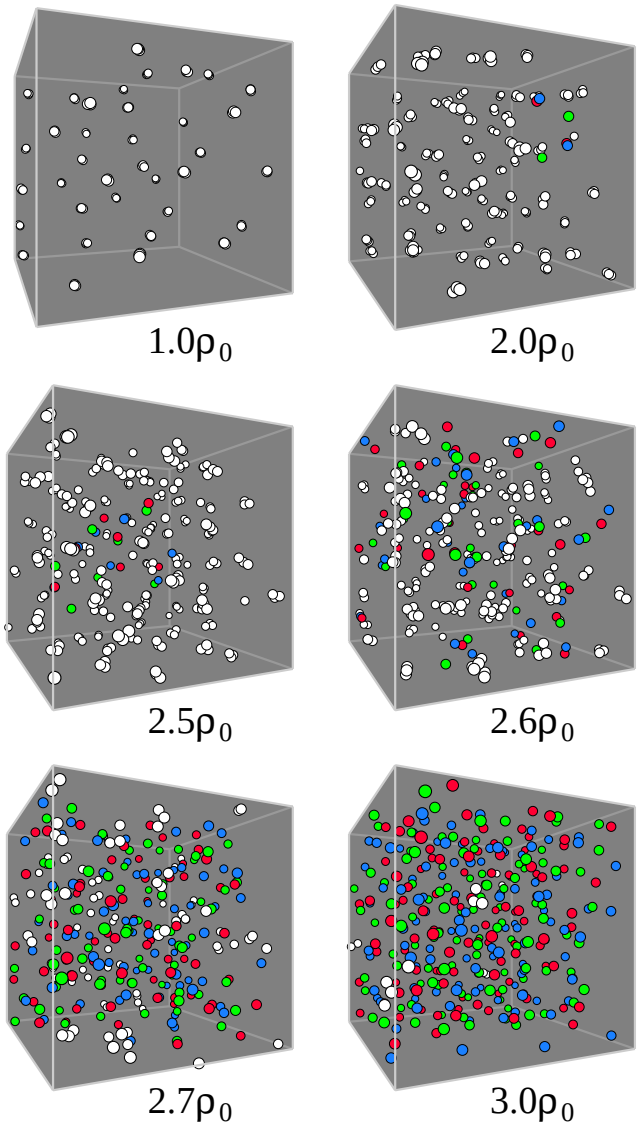

Fig. 3. Snapshots of *uds* matter with L=0.43 fm at various densities. Using the criterion of Eq. (15), confined quarks are plotted with white and deconfined quarks its own color. At $1\rho_0$ all quarks are confined. As the density increases deconfined quarks or its colors begin to appear. Most of the quarks are deconfined at $3\rho_0$.

the environment. In this way, the decrease of the kinetic energy is superior to the increase of potential energy.

In our result with the width parameter (I), the critical density is lower than that usually expected. The ground state energies by the width parameter (II) (L=0.33 fm) for *ud* and *udd* matters is shown in Fig. 5. The critical point of the baryon-quark transition is higher than that given by the width parameter (I). This implies that the transition occurs due to the density overlap of a quark with those in other baryons.

Figure 6 shows the energies for the three kinds of matters under the electric-charge neutral condition with the width parameter (I). The difference compared to Fig. 4 is that the energy of relativistic electron is added to the

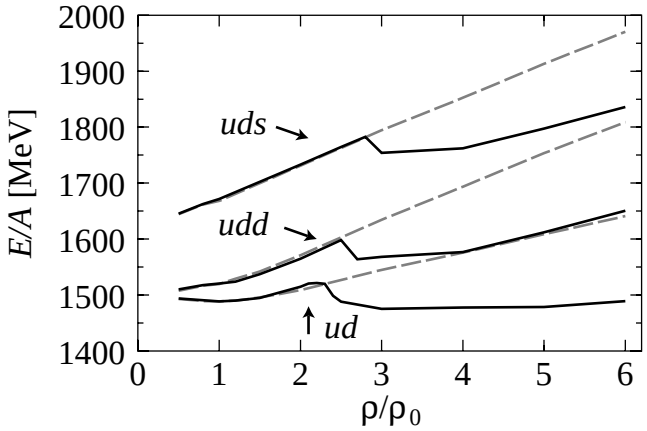

Fig. 4. Density dependence of energy per baryon for *ud*, *udd* and *uds* matter in case of width parameter (I) (L=0.43 fm). The dashed lines indicate the cases of baryon cooling and solid lines quark cooling.

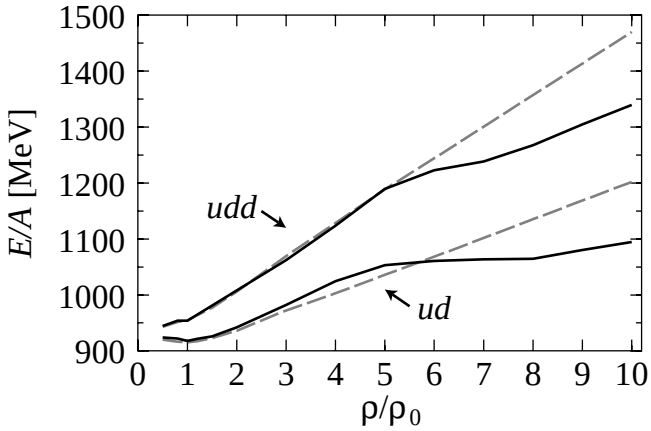

Fig. 5. The same figure as in Fig. 4, but with the width parameter (II) (L=0.33 fm).

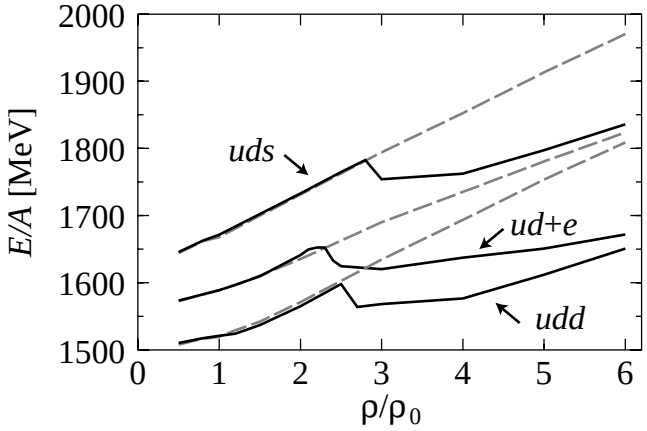

Fig. 6. Same as Fig. 4, but under the electric charge-neutral condition.

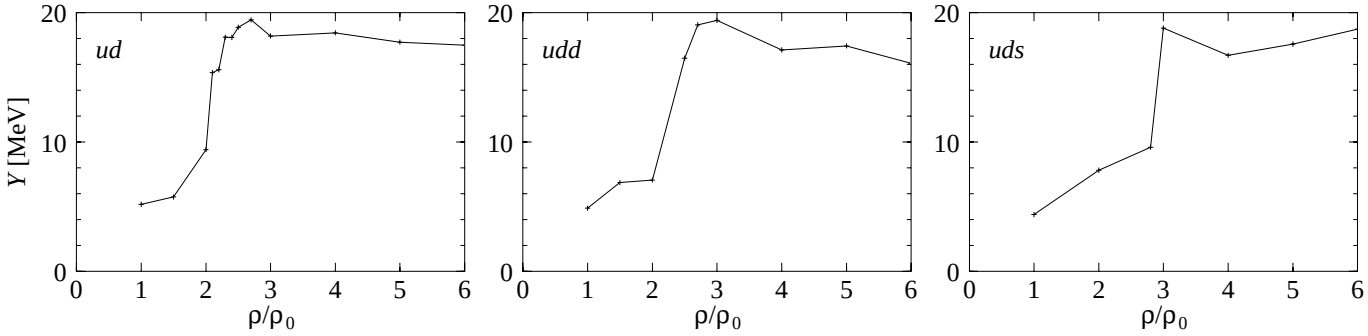

Fig. 7. Density dependence of Y for ud, udd and uds matter in case of width parameter (I) (L=0.43 fm).

energy of ud matter. Below $6\rho_0$ the energy of udd matter is the lowest. Judging from the behavior of the curves, however, ud matter becomes more stable than udd matter above $6\rho_0$.

The stability of strange matter has long been an attention of many nuclear and astrophysicists [28,29]. Our present result shows that uds matter is not favored even at high density. However, we cannot give a definite statement since our EOS of uds matter has ambiguity caused by ignorance of the Λ-Λ interaction. The width of s quarks and interactions concerning s quarks influence the stability as well.

Here we have examined these three kinds of fixed flavor matter for simplicity. For more realistic studies of matter realized in nature such as the core region of neutron stars, however, a simulation of matter in beta equilibrium is necessary. The most stable matter with non-integer u-d-s proportion would be close to udd matter at lower density, and between udd and ud matter at higher density. With the width parameter (I) there are density regions where the slope of E/A versus ρ/ρ_0 is negative in Fig. 6. Generally such a situation is not realized by forming non-uniform structure. In our case, however, the small size of the simulation box and the introduction of density-dependent parameters (13) caused this problem.

Now let us define a quantity Y which indicates the degree of deconfinement as, particle feels.

$$Y = \left(\left\langle \left| \sum_i^n V_{\rm color} \left(\mathbf{R}_i - \mathbf{R} \right) \right|^2 \right\rangle_{\mathbf{R}} \right)^{1/2} \tag{16}$$

where $\mathbf{R}$ is the position of a test particle in any color, $V_{\rm color}$ is the color potential which the test particle feels and $\langle\rangle_{\mathbf{R}}$ means the average over $\mathbf{R}$ which is sampled for 10000 points. If all quarks are confined in compact baryons, the value of Y becomes zero. Figure 7 shows the density dependences of Y. The value of Y is small at low density. From $2\rho_0$ to $3\rho_0$ which corresponds to the density region of baryon-quark transition, Y increases gradually. This gradual change of Y does not necessarily indicate the second order phase transition, since the mixed phase in the first order phase transition may also show the similar behavior of physical quantities.

4 extension to the finite temperature

4.1 Introduction of an effective temperature

We extend above MD to finite temperature systems. First of all, the definition of a temperature commonly used in MD is modified from the common expression due to the momentum-dependent Pauli potential according to Ref. [30],

$$\frac{3}{2} T_{\rm eff} = \frac{1}{n} \sum_{i=1}^{n} \frac{1}{2} \mathbf{P}_i \cdot \left(\frac{\partial H}{\partial \mathbf{P}_i} \right). \tag{17}$$

A popular method to control temperature in MD is known as Nosé-Hoover method [31]. The equilibrium is achieved by introducing an imaginary heat bath which interacts with a real system through an artificial coordinate and its momentum. The extended Hamiltonian for thermostat systems is written as

$$H_{\rm Nose} = H + \frac{1}{2} Q \xi^2 + 3 n T_{\rm set} \log w, \tag{18}$$

with $\xi = P_w / Q$, where w is an artificial variable, P_w is a momentum conjugate to w and Q corresponds to its mass. $T_{\rm set}$ is a target temperature of the system which is given as a parameter. The equations of motion are

$$\dot{\mathbf{R}}_i = \frac{\partial H_{\rm Nose}}{\partial \mathbf{P}_i} = \frac{\partial H}{\partial \mathbf{P}_i}, \tag{19}$$

$$\dot{\mathbf{P}}_i = -\frac{\partial H_{\rm Nose}}{\partial \mathbf{R}_i} = -\frac{\partial H}{\partial \mathbf{R}_i} - \xi \mathbf{P}_i, \tag{20}$$

$$\dot{w} = \frac{\partial H_{\rm Nose}}{\partial P_w} = \xi, \tag{21}$$

$$\dot{\xi} = \frac{3n}{Q} \left(T_{\rm eff} - T_{\rm set} \right). \tag{22}$$

Here $H_{\rm Nose}$ is conserved but the original effective Hamiltonian H fluctuates. The value of $T_{\rm eff}$ also fluctuates around $T_{\rm set}$ by the thermostat friction ξ.

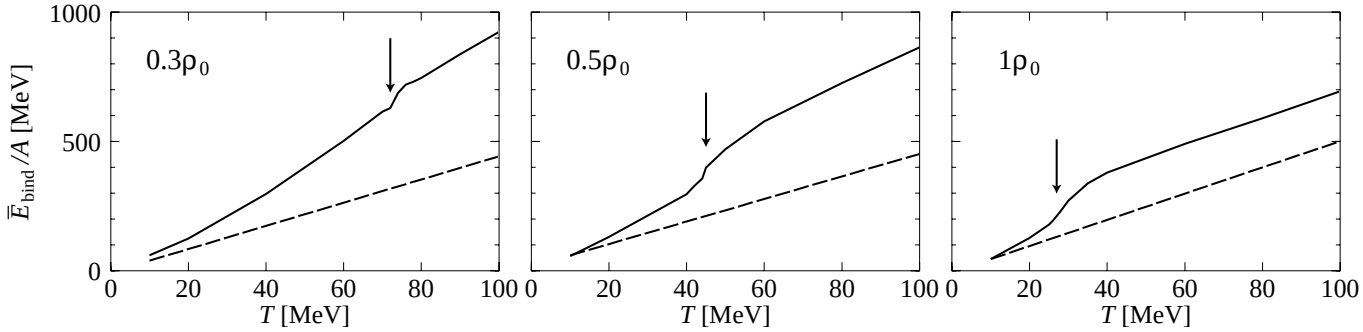

Fig. 8. Averaged binding energy per nucleon for ud matter with L=0.43 fm at $0.3\rho_0$ (left), $0.5\rho_0$ (center) and $1\rho_0$ (right) are shown with solid line. The dashed line denotes the case in which quarks are constrained to form baryons. The arrows indicate the critical temperature.

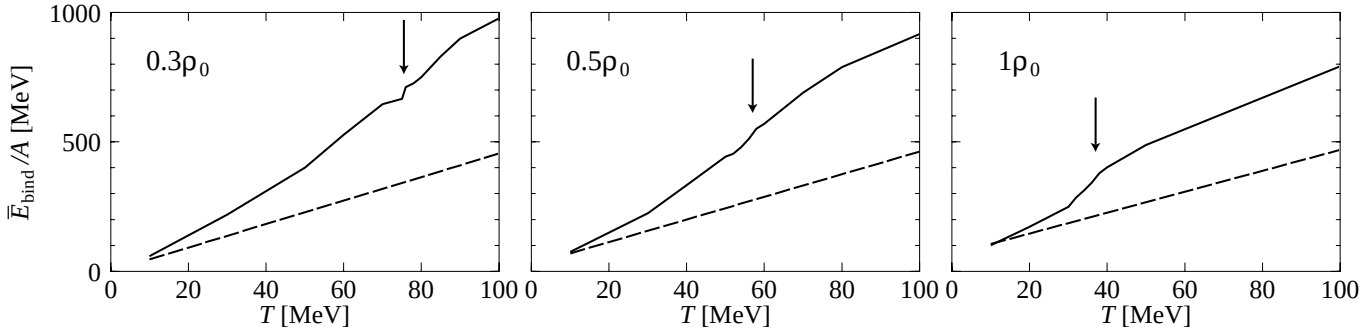

Fig. 9. The same figure as in Fig. 8, but for uds matter.

4.2 Results for the finite temperature system

We investigate the thermal property of quark matter for a wide range of density and temperature. Figure 8 shows temperature dependence of the averaged energy per baryon for ud matter at $0.3\rho_0$, $0.5\rho_0$ and $1\rho_0$ with $L = 0.43$ fm from the left by solid lines. Simulation results with the baryonization constraint are also shown by dashed lines for comparison. A baryon-quark transition can be seen as the change of specific heat. We define the critical temperatures by the maximum-specific-heat points and are indicated by arrows in this figure. The critical temperature becomes small as density increases. The lines without the baryonization constraint (normal calculation) disagree with those with the baryonization constraint because quarks can move in the baryon in case of normal calculations. The same quantity but for uds matter is shown in Fig. 9. The critical temperatures for uds matter are 5 – 15 MeV larger than that for ud matter at the same density. This is due to the presence of the s quarks having a larger mass than u and d quarks.

We draw a phase diagram by using our results of ud matter for L=0.43 fm in Fig. 10 and for L=0.33 fm in Fig. 11. Baryon phase is realized at lower side of density and temperature, and quark phase is realized at higher side in both diagrams, but baryon phase in Fig. 11 is larger than that of Fig. 10. This means that the quark width affects the phase transition due to the increase of temperature as well as the increase of den sity.

5 Summary

Quark many-body systems were studied by MD where the ground state was defined in a definite manner in terms of a Pauli potential. The EOS were reproduced for three kinds of baryon matters with effective meson exchange interactions between quarks. Baryon-quark transition is seen when baryon density increases. We have used two quark widths, $L = 0.43$ fm and $L = 0.33$ fm. The density at which baryon-quark phase transition occurs is different for the two widths since the transition is caused by the overlap of the quarks. In case of the larger value of $L = 0.43$ fm the baryon-quark transition occurs at rather low density, around $3\rho_0$. For $L = 0.33$ fm case, the transition occurs around $5\rho_0$, which is consistent with other theoretical calculations.

We have compared three kinds of matters with different u-d-s compositions: ud, udd and uds. Our results show that ud matter is the most stable among them and strange uds matter is not stable. For the EOS of uds or Λ matter, there would be still room for improvement to take into account the future experiment. For the color interaction, the color magnetic interaction is necessary as a color and flavor dependent interaction. The medium effects of constituent quark masses by the chiral symmetry restoration are also important to discuss the stability. A possibility to include the medium effect is to use the density dependent quark mass model (DDQM) [32]. However, the quark mass is derived there from the global density and is common for all quarks. This prescription may be too simple since the

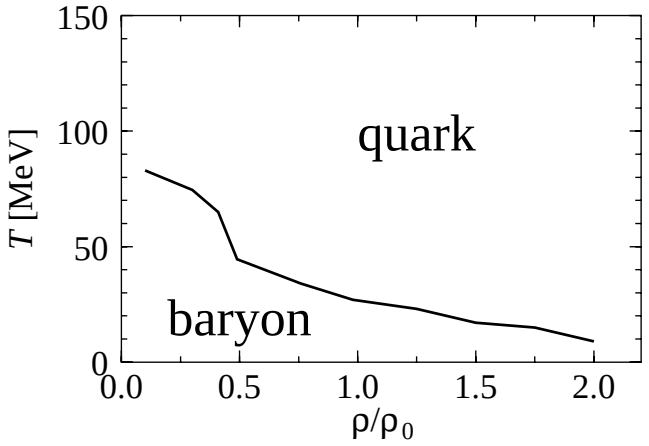

Fig. 10. Phase diagram with the density and temperature for ud matter in case of L=0.43 fm.

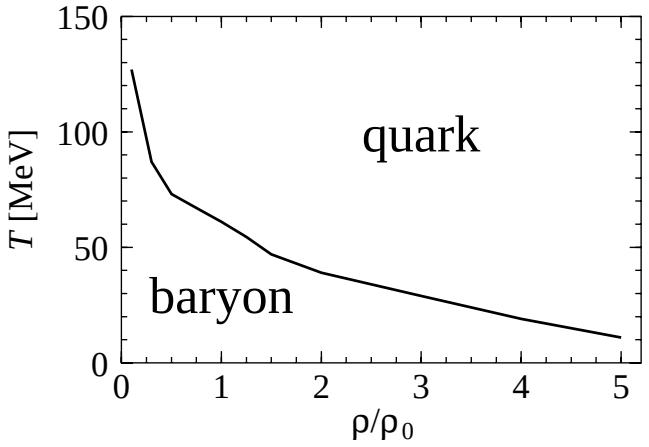

Fig. 11. Phase diagram with the density and temperature for ud matter in case of L=0.33 fm.

individual particle motion is essential in MD. A similar discussion can be done for the coupling constant α_s.

We have extended our model for the finite temperature systems. The baryon-quark transition can be seen as a change of specific heat. The critical temperature for uds matter is higher than ud matter by 5 – 15 MeV due to the heavy mass of s quark. Like the critical density, the critical temperature gets higher in case of L=0.33 fm than that of L=0.43 fm.

It is necessary to include $\bar{q}q$ creation/annihilation process for high temperature. Lack of antisymmetrization and the asymptotic freedom are also open problems.

Y. A. is grateful to T. Tanigawa, H. Koura, T. Tatsumi, T. Hatsuda, Y. Maezawa and T. Endo for their valuable discussions.

References

1. J. C. Collins and M. J. Perry, *Phys. Rev. Lett.* **34**, (1975) 1353 .
2. T. M. Schwarz, S. P. Klevansky and G. Papp, *Phys. Rev.* **C60**, (1999) 055205 .
3. J. B. Kogut and D. K. Sinclair, *Phys. Rev.* **D70**, (2004) 094501 .
4. A. Tawfik, *Phys. Rev.* **D71**, (2004) 054502 .
5. J. B. Kogut et al, *Phys. Rev. Lett.* **51**, (1983) 869 .
6. M. Stephanov, *Prog. Theor. Phys. Suppl.* **153**, (2004) 139 .
7. H. Satz, *Nucl. Phys.* **A642**, (1998) 130 .
8. M. C. Abreu et al., *Phys. Lett.* **B477**, (2000) 28 .
9. C. Adler et al., *Phys. Rev. Lett.* **89**, (2002) 132301 .
10. K. Suzuki et al., *Phys. Rev. Lett.* **92**, (2004) 072302 .
11. S. Ejiri, *Phys. Rev.* **D69**, (2004) 094506 .
12. Y. Nambu and G. Jona-Lasinio, *Phys. Rev.* **122**, (1961) 345 .
13. I. N. Mishustin, L. M. Satarov, H. Stöcker and W. Greiner, *Phys. Rev.* **C66**, (2002) 015202 .
14. J. Berger and C. V. Christov, *Nucl. Phys.* **A609**, (1996) 537 .
15. J. Aichelin *Phys. Rep.* **202**, (1991) 233 ; and references therein.
16. H. Feldmeier, *Nucl. Phys.* **A515**, (1990) 147 .
17. A. Ono, H. Horiuchi, T. Maruyama and A. Ohnishi, *Prog. Theo r. Phys.* **87**, (1992) 1185 .
18. T. Maruyama, K. Niita, and A. Iwamoto, *Phys. Rev.* **C53**, (1996) 297 .
19. A. Bonasera, *Phys. Rev.* **C60**, (1999) 065212 .
20. A. Bonasera, *Phys. Rev.* **C62**, (2000) 052202 .
21. M. Hofmann, et al., *Phys. Lett.* **B478**, (2000) 161 .
22. T. Maruyama and T. Hatsuda, *Phys. Rev.* **C61**, (2000) 062201.
23. T. Maruyama, K. Niita, K. Oyamatsu, T. Maruyama, S. Chiba and A. Iwam oto, *Phys. Rev.* **C57**, (1997) 655 .
24. T. Yoshimoto, T. Sato, M. Arima and T. S. H. Lee, *Phys. Rev.* **C61**, (2000) 065203 .
25. M. Papa, T. Maruyama and A. Bonasera, *Phys. Rev.* **C64**, (2001) 024612 .
26. S. Terranova and A. Bonasera, *Phys. Rev.* **C70**, (2004) 024906 .
27. H. Q. Song, R. K. Su, D. H. Lu and W. L. Qian, *Phys. Rev.* **C68**, (2003) 055201 .
28. A. R. Bodmer, *Phys. Rev.* **D4**, (1971) 1601 .
29. E. Witten, *Phys. Rev.* **D30**, (1984) 272 .
30. G. Watanabe, K. Sato, K. Yasuoka and T. Ebisuzaki, *Phys. Rev.* **C69**, (2004) 055805 .
31. W. G. Hoover, *Phys. Rev.* **A31**, (1985) 1695 .
32. Z. Xiaoping, L. Xuewen, K. Miao and Y. Shuhua, *Phys. Rev.* **C70**, (2004) 015803 .